Cellular and Molecular Life Sciences (2022) 79:72
https://doi.org/10.1007/s00018-021-04114-z

ORIGINAL ARTICLE

Agonist-induced extracellular vesicles contribute to the transfer of functional bombesin receptor-subtype 3 to recipient cells

Zeyuan Wang[1] · Lehao Wu[1] · Huiyu Wang[1] · Yan Zhang[2] · Hua Xiao[1]

Received: 4 August 2021 / Revised: 21 December 2021 / Accepted: 22 December 2021 / Published online: 15 January 2022

Abstract

Extracellular vesicles (EVs) are important carriers for biomolecules in the microenvironment that greatly promote intercellular and extracellular communications. However, it is unclear whether bombesin receptor-subtype 3 (BRS-3), an orphan G-protein coupled receptor, can be packed into EVs and functionally transferred to recipient cells. In this study, we applied the synthetic agonist and antagonist to activate and inhibit the BRS-3 in HEK293-BRS-3 cells, whose EVs release was BRS-3 activation dependent. The presence of BRS-3 in harvested EVs was further confirmed by an enhanced green fluorescent protein tag. After recipient cells were co-cultured with these EVs, the presence of BRS-3 in the recipient cells was discovered, whose function was experimentally validated. Quantitative proteomics approach was utilized to decipher the proteome of the EVs derived from HEK293-BRS-3 cells after different stimulations. More than 900 proteins were identified, including 51 systematically dysregulated EVs proteins. The Ingenuity Pathway Analysis (IPA) revealed that RhoA signaling pathway was as an essential player for the secretion of EVs. Selective inhibition of RhoA signaling pathway after BRS-3 activation dramatically reversed the increased secretion of EVs. Our data, collectively, demonstrated that EVs contributed to the transfer of functional BRS-3 to the recipient cells, whose secretion was partially regulated by RhoA signaling pathway.

Keywords Vesicles · Orphan GPCR · Proteomics · RhoA signaling pathway

Introduction

Extracellular vesicles (EVs) are nanoscale particles released by most types of cells in an evolutionally conserved manner, and they are encapsulated by lipid bilayers [1]. According to the minimal information for studies of extracellular vesicles 2018 (MISEV2018), EVs are mainly categorized as two subtypes according to their physical characteristics, namely, small EVs (sEVs) (< 200 nm) and medium/large EVs (m/lEVs) (> 200 nm) [2]. They present in different body fluids, such as blood, urine, and saliva [3, 4]. The secretion of EVs was originally described as a process for cells to eliminate unneeded biomolecules [5]. However, during the past 2 decades, scientists have discovered that EVs may act as potent mediators in intercellular communications as well as extracellular microenvironment [6]. Due to their capacity to exchange nucleic acids, proteins, lipids, and metabolites, EVs can transmit signaling molecules among cells, influence the pathological and physiological state of parental and recipient cells, and participate in the development of various diseases [7]. Moreover, both natural and engineered EVs have been utilized as drug delivery nano-carriers, cancer vaccines, detection markers, and therapeutic agents or targets in diseases, especially in cancers [8]. Proteomics technology has been employed for the large-scale analysis of EVs proteome [9]. Among the proteins harbored by EVs, some G-protein coupled receptors (GPCRs) could also be identified [10].

GPCRs usually contain seven transmembrane domains and constitute the largest family of proteins in the

Zeyuan Wang and Lehao Wu contributed equally as first authors to this work.

✉ Yan Zhang
zhangyan_sjtu@sjtu.edu.cn

✉ Hua Xiao
huaxiao@sjtu.edu.cn

[1] State Key Laboratory of Microbial Metabolism, Joint International Research Laboratory of Metabolic and Developmental Sciences, School of Life Sciences and Biotechnology, Shanghai Jiao Tong University, Shanghai 200240, China

[2] School of Pharmacy, Shanghai Jiao Tong University, Shanghai 200240, China

mammalian genome, including approximately 800 members [11]. GPCRs have attracted long-standing interests as drug targets, largely because they mediate cell signaling, regulate numerous physiological processes, and contain druggable sites accessible on the cell surface [12]. For many of these GPCRs, one or several endogenous ligands have been identified. However, there are some GPCRs that have not been decisively paired with their endogenous ligands, which are classified as "orphan" GPCRs [13]. For instance, Bombesin receptor-subtype 3 (BRS-3) is an orphan receptor, whose endogenous ligands have not been found till now [14]. Because of its 51% and 47% homology to the other two mammalian bombesin receptors, BRS-3 is categorized as a member of the bombesin receptor family [15, 16], which is widely expressed in the central nervous system, peripheral tissues, and gastrointestinal tract [17, 18]. It plays critical roles in the regulation of insulin secretion, energy expenditure, body temperature and heart rate, and is, therefore, involved in a number of human diseases such as asthma and kidney diseases [18–20]. In-depth study on BRS-3 may reveal new insights into potential treatments of related diseases.

Ligand-activated receptors go through rapid desensitization and endocytosis and are subsequently internalized into early endosomes [21]. In general, there are few typical fates for GPCRs in cells, which proceed through respective pathways. As a representative fate, some GPCRs can be recycled rapidly and efficiently, and then sent back to the plasma membrane. These re-used GPCRs may respond again to the stimulation of its ligands [22]. This process is called re-sensitization. As another general fate, some GPCRs may be sorted into multi-vesicular bodies, followed by lysosomal degradation, a process guided by ubiquitination [23]. Moreover, recent studies show that very few GPCRs may be packed into EVs and transferred to recipient cells functionally. For example, when Angiotensin II Type 1 receptor (AT1R) is activated by mechanical stress or its ligand, host cells release exosomes that containing functional AT1R. AT1R-enriched exosomes may target cardiomyocytes, skeletal myocytes and mesenteric resistance vessels, and modulate blood pressure responses in vivo [24]. However, it is unclear whether functional BRS-3 can be sorted into EVs after activation and transferred to recipient cells.

Quantitative proteomics is a powerful tool for comprehensive proteome analysis in biomedical research, including BRS-3 research and EVs discovery. In our previous study, a dynamic protein profiling of HEK293-BRS-3 cells after BRS-3 activation was analyzed, which demonstrated that BRS-3 activation had essential impact on cell death and survival, protein synthesis, as well as mRNA translation. Activation of BRS-3 might enhance mTOR pathway and further promoted cell proliferation [25]. By utilizing tandem mass tags based quantitative proteomics, we found that EVs derived from highly metastatic lung cancer cells carried high level of hepatocyte growth factor (HGF), activating the HGF/c-Met pathway in recipient cells and promoting their metastasis [26]. Through characterizing the protein profiling in EVs from HEK293-BRS-3 cells by quantitative proteomics, we might reveal the potential fate of BRS-3 and its related key pathways.

In this study, we hypothesized that BRS-3 could be packed into EVs and released to the microenvironment, which would be further utilized by recipient cells. A synthetic agonist of BRS-3 was used to activate the receptor on HEK-293T cells and secreted EVs in the culture media were monitored. The presence of BRS-3 was evaluated in the harvested EVs through labeling with an enhanced green fluorescent protein (eGFP) tag. After confirmation, these labeled EVs were further incubated with recipient cells. The presence of BRS-3 in recipient cells was measured and its function was tested with agonist activation and inhibition, followed by detecting the phosphorylation of ERK protein. Quantitative proteomics was used to compare the protein profiling in secreted EVs before and after activation and inhibition. Key pathways that related to the secretion of EVs were revealed. Selected signaling pathway was further validated and the potential mechanism for EVs' fate was discussed.

Materials and methods

Chemicals and reagents

[Dphe^{6}, βAla^{11}, Phe^{13}, Nle^{14}] Bn (6–14), namely Pep #1, was purchased from Guoping Biotechnology Co. Ltd. (Anhui, China). Boc-Phe-His-4-amino-5-cyclohexyl-2,4,5-trideoxypentonyl-Leu-(3-dimethylamino) benzyl amide-*N*-methylammonium trifluoroacetate, namely Bantag-1, was kindly provided by Professor Olivier Civelli at University of California, Irvine. Y-27632 was purchased from Beyotime Biotechnology (catalog no. SC0326). Antibodies for phosphor-ERK, ERK, and Calnexin were purchased from Cell Signaling Technology (catalog no. 9101, 4695, 2679). Antibodies for TSG101 and CD63 were purchased from Abcam (catalog no. ab125011, ab217345).

Cell culture and establishment of transfectants

HEK293-BRS-3 stable cells were a generous gift from Professor Olivier Civelli at University of California, Irvine. HEK-293T cells were purchased from the American Type Culture Collection (ATCC). HEK293-BRS-3 cells and HEK-293T cells were cultured in Dulbecco's Modified Eagle Medium (DMEM, Thermo Fisher Scientific INC.) supplemented with 10% fetal bovine serum (FBS, Gibco), 100

units/mL penicillin, and 100 mg/mL streptomycin (Gibco). Cells were incubated at 37 °C under a humidified atmosphere of 5% CO_2. For transfection in HEK-293T cells, One-Step DNA Transfecter Kit (Enlighten Biotech) was used according to the manufacturer's protocol. The plasmid of BRS-3-eGFP was pcDNA3.1(+) BRS-3-eGFP.

EVs isolation

Prior to agonist stimulation and isolation of EVs, cells were washed with PBS one time. The agonist, antagonist, and selected inhibitor were dissolved in the medium only containing DMEM, i.e. EVs were separated from the medium without FBS. After cell culture and different treatments, the culture medium was collected for EVs isolation through differential centrifugation. To remove impurities, the culture medium was initially centrifuged at 300 *g* for 10 min, 2000 *g* for 10 min, 10,000 *g* for 20 min. Then the supernatants were ultra-centrifuged at 100,000 *g* for 70 min (Optima Max Ultracentrifuge, Beckman Coulter) to precipitate EVs. All sample preparation was performed at 4 °C.

Nanoparticle tracking analysis (NTA)

The concentration and size of EVs were measured by Nano Particle Tracking systems, including NanoSight (NS300, Malvern) and ZetaView (Zeta potential distribution Analyzer, Particle Metrix). NanoSight and ZetaView were used for the measurement of EVs' concentration and size distribution, and their instrument parameter settings were as follows: ZetaView (software version ZetaView 8.05.04)—sensitivity 70, shutter 70; NanoSight (software version NanoSight NTA 3.4)—camera level 12–13, slider shutter 1200–1232, slider gain 146–219. ZetaView was used for the detection of EVs' eGFP, and the instrument parameter settings were as follows: ZetaView (software version ZetaView 8.05.04)—sensitivity 87, shutter 100. EVs were re-suspended in PBS, and then injected into the sample chamber. Each sample was measured according to the manufacturer's instructions.

Transmission electron microscopy (TEM)

The morphology of EVs was checked by Philips CM120 transmission electron microscope (Eindhoven, Netherlands), which operated at 120 kV. 10 μL of re-suspended EVs solution was loaded onto an ultrathin carbon film 300 mesh copper grid, which was dried for fixation, then stained with 2% phosphotungstic acid.

Protein sample preparation and western blotting

HEK293-BRS-3 cells and EVs were lysed with RIPA buffer (Beyotime Biotechnology, catalog no. P0013B) containing phenylmethanesulfonyl fluoride (PMSF, Beyotime Biotechnology, catalog no. ST506). Protein concentration was measured by the bicinchoninic acid method (BCA method, Thermo Fisher Scientific INC.). SDS-PAGE Sample Loading Buffer (Beyotime Biotechnology, catalog no. P0015) was added to the lysate and heated at 99 °C for 10 min. HEK-293T cells were plated into 24-well plates and incubated with harvested EVs for 12 h, then stimulated by BRS-3 agonist (Pep #1) or antagonist (Bantag-1). Proteins were collected by adding SDS–PAGE Sample Loading Buffer and heated at 99 °C for 10 min.

The protein samples were loaded onto a 10% SDS–PAGE, separated, and then transferred to polyvinylidene-fluoride membrane (PVDF, Merck Millipore). ECL (PerkinElmer, catalog no. NEL104001) was used for visualization. The protein bands were quantified using the NIH Image J software (NIH, Bethesda, MD).

Flow cytometry

HEK293-BRS-3 cells were seeded in 10 cm diameter dishes. After the cells grew and reached 95% confluence, Pep #1 was added with DMEM into dishes. The EVs were isolated from the culture medium using ultracentrifugation method, which were re-suspended in DMEM with 10% FBS. The EVs were further added to HEK-293T cells for incubation. After cultured with EVs for 12 h, HEK-293T cells were harvested with trypsin–EDTA (Gibco), washed with PBS twice, followed by centrifugation at 300 *g* for 3 min at 4 °C twice. The collected cells were re-suspended in PBS for flow cytometry analysis (BD LSR FORTESSA, BD Biosciences). The percentage of FITC-A in cells was analyzed with the FlowJo software (Tree Star, Inc., San Carlos, CA, USA).

LC–MS/MS

Extracted EVs proteins were digested overnight at 37 °C by trypsin (Promega, V5071) through using FASP approach [27]. Briefly, HEK293-BRS-3 cells were seeded into 15 cm diameter dishes. After the cells grew and reached 95% confluence, DMSO, Pep #1, Bantag-1 (BT1), or BT1 + Pep #1 dissolved in DMEM were added, respectively. EVs proteins obtained from different treatment groups were processed and three technical repeats were prepared for each group. After desalting, digested peptides were analyzed with Easy-nanoLC1000 coupled with an Orbitrap Q-Exactive Plus Mass spectrometer (Thermo Fisher Scientific, Waltham, Massachusetts). A 15 cm × 50 μm reverse-phase column (2 μm, C18, 120 Å, Thermo Fisher Scientific INC.) was utilized for the separation of peptides. The mobile phases were Buffer A (0.1% formic acid in water) and Buffer B (80% acetonitrile with 0.1% formic acid). The gradient was: 2–20% Buffer B in 98 min, 20–30% in 10 min, 30–95% in 2 min, and

then kept at 95% for 8 min, 95–2% in 1 min, and sustained for 1 min at 2%. The flow rate was 300 nL/min. The MS scan was ranged from 350 to 1500 *m/z* with 70,000 resolution. For MS/MS, the scan was ranged from 200 to 2000 *m/z* with 17,500 resolution. The raw data were submitted for database search by MaxQuant (version 1.6.1.0) software, which searched against UniProt Human database (release 2017_11_28, 20,244 entries). Up to two missed cleavages was permitted. Trypsin was selected as the enzyme for protein digestion. Cysteine carbamidomethylation was set as a fixed modification, and methionine oxidation, N-terminal acetylation were set as variable modifications. Maximum peptide and protein false discovery rates (FDR) were both limited to 1%. Label-free quantification was performed by Intensity-based absolute quantification (iBAQ). Quantile normalization was performed to ensure each sample had the same distribution. The criteria of at least two unique peptides, 1.5-fold change (FC), and p value < 0.05 were applied for the screening of differentially expressed proteins.

Bioinformatics and statistical analysis

Omicsbean (http://www.omicsbean.com/) was used for KEGG pathway analysis. Ingenuity Pathway Analysis (IPA, Ingenuity Systems, QIAGEN, http://www.ingenuity.com) of identified proteins were used to discover "Canonical Pathways".

The experimental results were represented as the mean ± SEM (standard error of measurement). The comparisons of quantitative data between two groups were assessed using the t test, and $p < 0.05$ was considered as statistical significance. All statistical analyses were performed by the GraphPad Prism 9 (San Diego, CA, USA).

Results

Induction of EVs secretion by the activation of BRS-3 in HEK293-BRS-3 cells

The workflow of this study is shown in Fig. 1a. We used ultracentrifugation to isolate EVs, which were then characterized by TEM, NTA, and western blotting. Figure 1b shows the TEM of isolated EVs from HEK293-BRS-3 cells after activation. The size distribution of the cup-shaped EVs ranged from 30 to 600 nm (Fig. 1c). TSG101 and CD63, representative markers of EVs, were well detected in these isolated EVs, while negative marker like Calnexin was negligible (Fig. 1d). These results demonstrated that EVs were successfully obtained from cell cultural media.

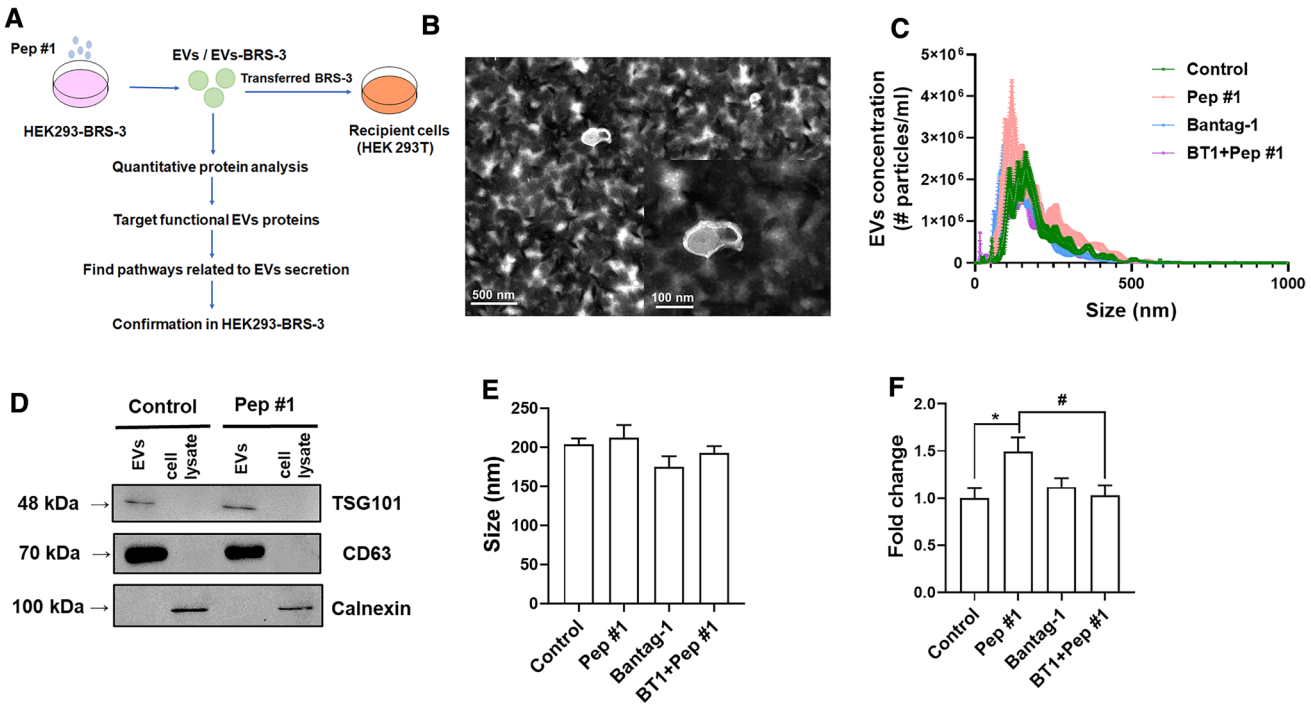

Fig. 1 Activation of HEK293-BRS-3 cells increases EVs secretion. **a** Workflow of this work. **b-d** Characterization of EVs isolated from HEK293-BRS-3 cells with or without activation by TEM (**b**), NTA (**c**), and immunoblotting (**d**). Western blots of EVs and cell lysates for typical markers TSG101, CD63, and the cellular marker Calnexin. **e–f** Mean size(**e**) and fold change (**f**) of EVs from HEK293-BRS-3 cells with different treatments (DMSO, Pep #1, Bantag-1 or BT1 + Pep #1) by NTA (n = 10). *, $p < 0.05$ versus control; #, $p < 0.05$ versus BT1 + Pep #1 by t test

Then, we used NanoSight to measure the concentration and mean size of EVs. As shown in Fig. 1e, the mean size of EVs secreted by HEK293-BRS-3 cells was around 200 nm. Activation and inhibition of BRS-3 had minor effect on the size of EVs. However, we found that the amount of EVs secreted by HEK293-BRS-3 cells increased approximately 50% (Fig. 1f), once the BRS-3 was activated by its synthetic agonist Pep #1 (10 μM) for 30 min. Interestingly, the increase of EVs secretion induced by Pep #1 was dramatically reversed by the addition of 1 nM Bantag-1, a specific antagonist against BRS-3 (Fig. 1f) [28]. Meanwhile, the addition of Bantag-1 alone had only minor effect on EVs secretion. These data demonstrated that activation of BRS-3 in HEK293-BRS-3 cells could increase their secretion of EVs.

Packaging of BRS-3 into EVs

To confirm the presence of BRS-3 in cells, we used a plasmid, BRS-3-eGFP, to track its green fluorescent labeling. The sequence of BRS-3-eGFP plasmid is shown in Fig. S1. BRS-3-eGFP was observed in cells, which verified that BRS-3 had been successfully transfected into HEK-293T cells (Fig. 2a–c). Then we tested whether the transfected BRS-3-eGFP was functional in the cells by detecting their ability to phosphorylate ERK [29]. In HEK-293T cells transfected with BRS-3-eGFP, we found that the phosphorylation of ERK was significantly increased when the cells were stimulated with Pep #1 (Fig. 2d, e). More importantly, this phenomenon was reversed by Bantag-1 (Fig. 2d, e). Meanwhile, we transfected BRS-3-eGFP and BRS-3 plasmids into HEK-293T cells, respectively. By detecting the phosphorylation of ERK, we found that the tag of GFP did not affect BRS-3 signaling (Fig. S2). Using confocal fluorescent microscope, we discovered that GFP fusion with the BRS-3 did not affect the receptor's cell localization and cycling (Fig. S3). Therefore, we confirmed that BRS-3 was functional in these transfected HEK-293T cells.

To demonstrate the presence of BRS-3 in cell secreted EVs, we used Pep #1 to stimulate cells with transfected BRS-3-eGFP and isolate their derived EVs. DMSO treatment was used as a control. The size distribution and concentration of all EVs in each group were analyzed by ZetaView. As shown in Fig. 2f, for the cells transfected with BRS-3-eGFP, the amount of their secreted EVs was increased after Pep #1 stimulation when compared with the DMSO treatment group. Majority of their size was less than 300 nm. This result was consistent with that in Fig. 1f. Then

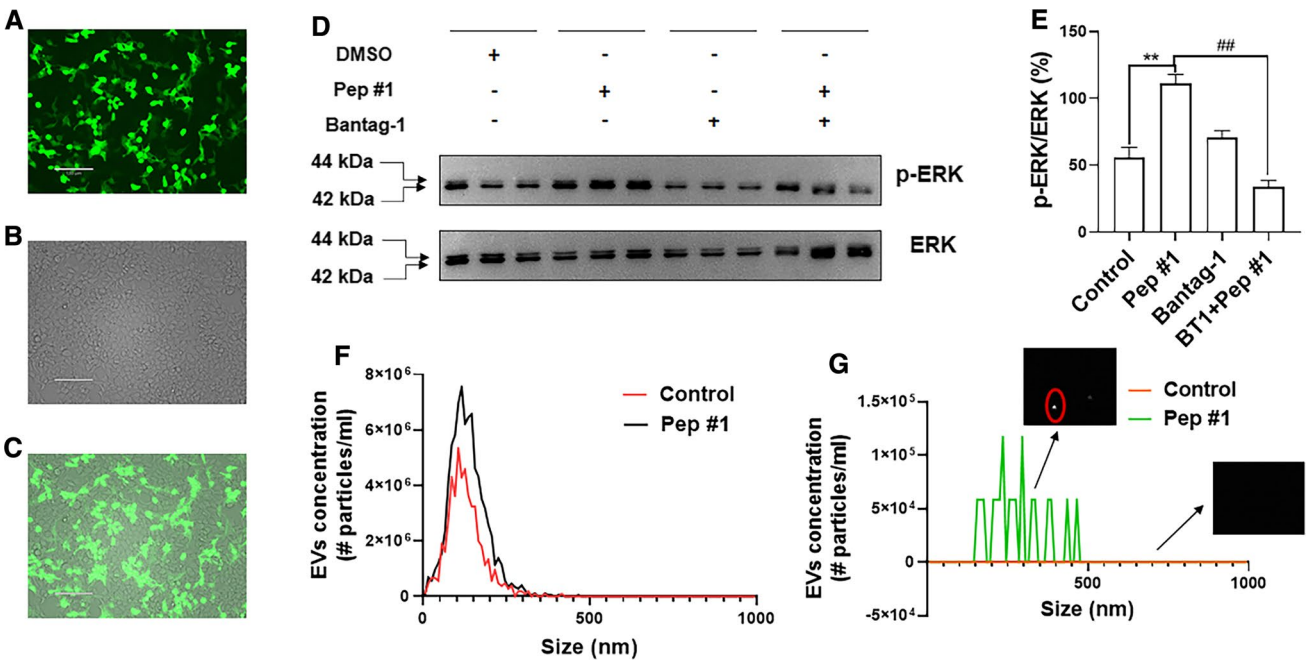

Fig. 2 EVs derived from HEK293-BRS-3 cells after activation contain BRS-3. **a–c**, HEK-293T cells were transfected with BRS-3-eGFP plasmid. Cells were photographed using fluorescence microscope (**a**) and light microscope (**b**). These two pictures were merged (**c**). The scale bar in the panel is 130 μm. **d–e** Effect of Pep #1 and Bantag-1 induced phosphorylation of ERK in HEK-293T cells transfected with BRS-3-eGFP plasmid. Cells were stimulated by Pep #1 (10 μM) for 1 min, or Bantag-1 (1 μM) for 10 min and Pep #1 (10 μM) for 1 min. Quantification of the p-ERK (**e**) ($n=3$). **, $p<0.01$ versus control; ##, $p<0.05$ versus BT1 + Pep #1 by t test. **f** Total EVs derived from HEK-293T cells that transfected with BRS-3-eGFP plasmid with (black line) or without (red line) stimulation of Pep #1. **g** Fluorescent EVs derived from HEK-293T cells that transfected with BRS-3-eGFP plasmid with (green line) or without (orange line) stimulation of Pep #1 (10 μM)

we measured the fluorescence intensity of BRS-3-eGFP in these isolated EVs. For the cells treated with DMSO, no fluorescence could be observed from their derived EVs (Fig. 2g). However, after the cells were stimulated by Pep #1, abundant fluorescent signals could be detected in their secreted EVs. The size distribution of the EVs ranged from 150 to 500 nm. These data suggested that EVs secreted by HEK-293T cells (which transfected with BRS-3-eGFP) contained BRS-3, after the activation of BRS-3 by its agonist.

BRS-3 transferred to recipient cells by EVs are biochemically functional

Flow cytometry was used to demonstrate whether EVs could transfer BRS-3 into the recipient cells. For HEK-293T cells transfected with BRS-3-eGFP, their cultural media were harvested for the isolation of EVs, which were further co-cultured with HEK-293T cells for 12 h. When compared with HEK-293T cells co-cultured with EVs derived from the cells with DMSO stimulation, increased fluorescence intensity was observed for the HEK-293T cells co-cultured with EVs derived from cells with Pep #1 stimulation (Fig. 3a, right panel). The quantification results are shown in Fig. 3b. The presence of BRS-3-eGFP in HEK-293T cells demonstrated that BRS-3 was transferred to the recipient cells by EVs.

To determine whether the BRS-3 transferred by EVs was functional in the recipient cells, we measured ERK phosphorylation in HEK-293T cells after the incubation with EVs isolated from the cultural media of the HEK293-BRS-3 cells stimulated with Pep #1. Stimulation of HEK-293T cells by Pep #1 for 1 min resulted in the significant increase of ERK1/2 phosphorylation when compared with the DMSO control. This phenomenon was completely blocked by the pretreatment with Bantag-1 (Fig. 3c, d). These results illustrated that EVs had transferred BRS-3 into HEK-293T cells which could activate agonist dependent signaling. Therefore,

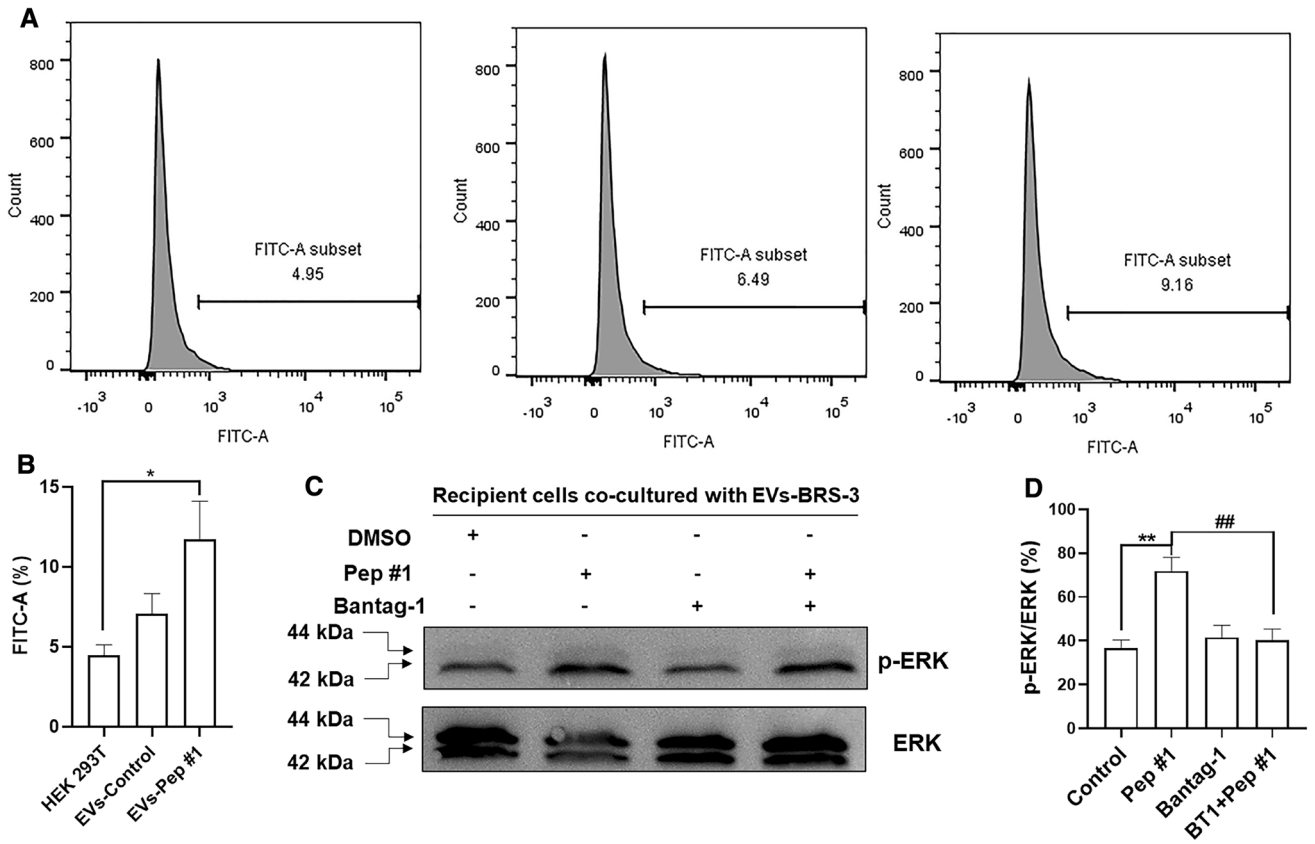

Fig. 3 BRS-3 transferred by EVs are functional. **a** Flow cytometry of HEK-293T cells. HEK-293T cells were co-cultured with EVs, which came from HEK-293T cells transfected with BRS-3-eGFP plasmid with or without Pep #1 stimulation (10 μM). Left panel: HEK-293T cells, middle panel: HEK-293T cells co-cultured with EVs derived from cells without stimulation, right panel: HEK-293T cells co-cultured with EVs derived from cells with Pep #1 stimulation. **b** Quantification of the FITC-A (n = 5). *, $p < 0.05$ versus HEK-293T by *t* test. **c** Effect of HEK-293T cells on Pep #1 induced phosphorylation of ERK. HEK-293T cells preincubated with EVs derived from culture media of HEK293-BRS-3 cells with Pep #1 stimulation. Then HEK-293T cells were stimulation with Pep #1 (10 μM) for 1 min, or Bantag-1 (1 μM) for 10 min and Pep #1 (10 μM) for 1 min. **d** Quantification of the p-ERK (n = 4). **, $p < 0.01$ versus control; ##, $p < 0.05$ versus BT1 + Pep #1 by *t* test

the BRS-3 transferred to recipient cells by EVs were biochemically functional.

Proteomics analysis of the EVs derived from the HEK293-BRS-3 cells after activation or inhibition

Quantitative proteomics analysis of EVs was performed to identify potential signal pathways for BRS-3. Proteins of the EVs isolated from the culture media of the HEK293-BRS-3 cells with different treatments (DMSO, Pep #1, Bantag-1, BT-1 + Pep #1) were analyzed by LC–MS/MS in parallel, and three technical replicates were prepared for each treatment group. In total, 911 proteins were identified from these EVs, among which 477 proteins (52.4%) were shared by four groups (Fig. 4a). More specifically, 48 (5.3%), 78 (8.6%), 32 (3.5%), 41 (4.5%) proteins were uniquely identified in DMSO, Pep #1, Bantag-1, BT1 + Pep #1 groups, respectively (Fig. 4a). As the volcano plots shown in Fig. 4b, 122 proteins were upregulated and 68 proteins were

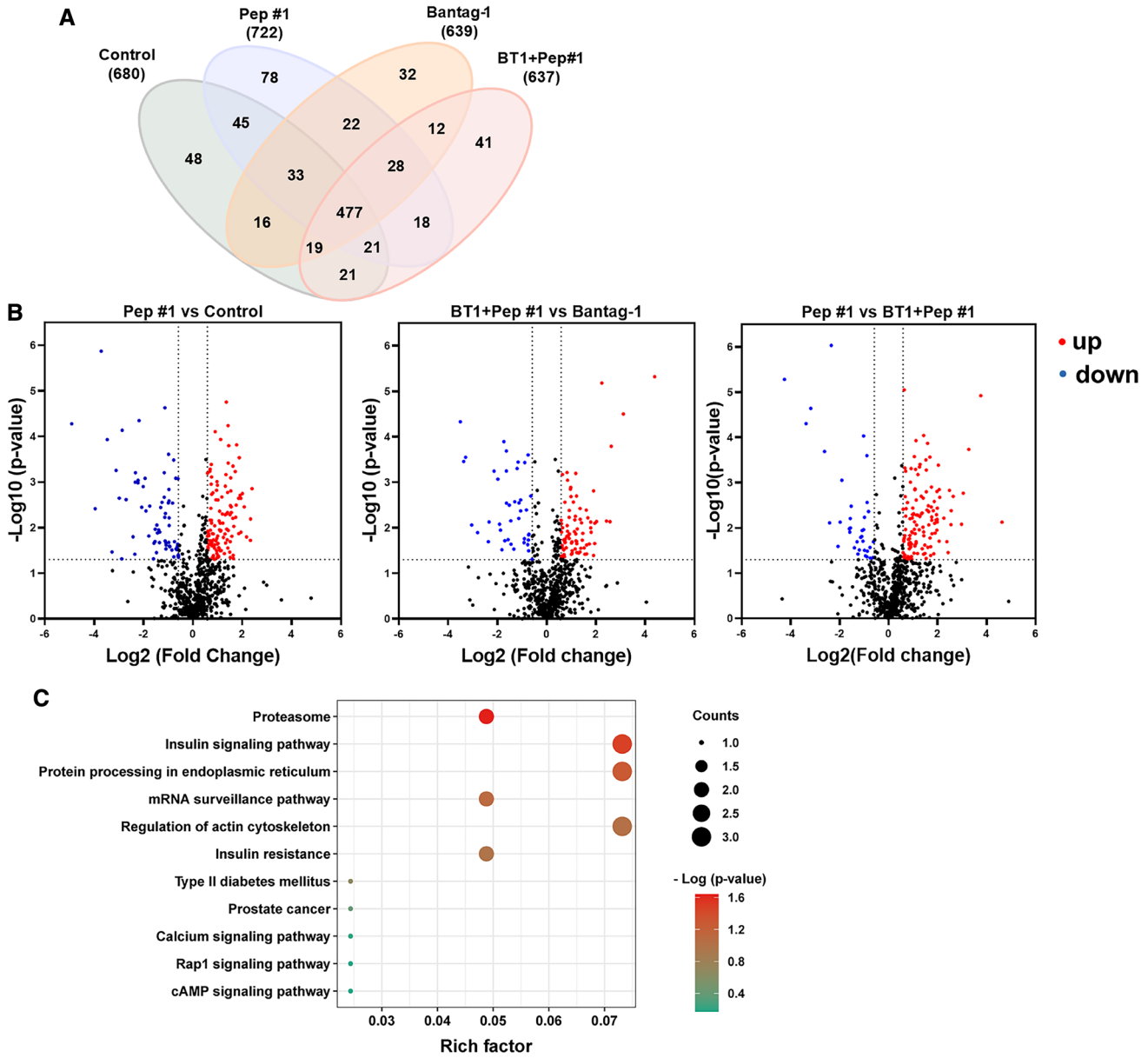

Fig. 4 Qualitative and quantitative analysis of EVs' proteome from different treatments. **a** Venn diagram of the EVs proteome from HEK293-BRS-3 cells treated with DMSO (Control), Pep #1, Bangtag-1 (BT1), BT1 + Pep #1. **b** Volcano plots of the proteomes in Pep #1 group compared with DMSO (Control) group (left panel), BT1 + Pep #1 group compared with Bantag-1 group (middle panel), and Pep #1 group compared with BT1 + Pep #1 group (right panel). **c** KEGG pathways involved in BRS-3 and EVs

Table 1 Fold change of 51 systematically dysregulated EVs proteins

No	Protein name	Protein ID	Pep #1/Control	BT1 + Pep #1/Pep #1
1	Carboxypeptidase D	O75976	> 100.00	0.8742
2	Insulin receptor substrate 4	O14654	5.2604	0.5475
3	EMILIN-2	Q9BXX0	5.0388	0.5328
4	Poly [ADP-ribose] polymerase 1	P09874	3.4065	0.3492
5	Citrate synthase, mitochondrial	O75390	3.2820	0.2548
6	Leucine–tRNA ligase, cytoplasmic	Q9P2J5	3.0657	0.5613
7	DNA-dependent protein kinase catalytic subunit	P78527	2.9286	0.5594
8	T-complex protein 1 subunit zeta	P40227	2.8920	0.8462
9	Splicing factor 3A subunit 1	Q15459	2.8686	0.4592
10	LIM and senescent cell antigen-like-containing domain protein 1	P48059	2.8480	0.5521
11	Heterogeneous nuclear ribonucleoprotein M	P52272	2.7023	0.2626
12	X-ray repair cross-complementing protein 6	P12956	2.6945	0.6175
13	X-ray repair cross-complementing protein 5	P13010	2.6865	0.6098
14	Coatomer subunit alpha	P53621	2.6694	0.5186
15	Proteasome subunit alpha type-2	P25787	2.6223	0.8207
16	Threonine–tRNA ligase 1, cytoplasmic	P26639	2.5798	0.3301
17	Serine/threonine-protein phosphatase PP1-beta catalytic subunit	P62140	2.5534	0.4644
18	ATP-dependent 6-phosphofructokinase, platelet type	Q01813	2.5293	0.4764
19	Protein disulfide-isomerase A3	P30101	2.2842	0.3374
20	Annexin A4	P09525	1.7200	0.7317
21	Unconventional myosin-Ic	O00159	2.2113	0.2582
22	Histone H2A type 1-J	P0C0S5	2.1811	0.7951
23	Chloride intracellular channel protein 1	O00299	2.1799	0.3976
24	Heterogeneous nuclear ribonucleoproteins C1/C2	P07910	2.1757	0.6150
25	Heterogeneous nuclear ribonucleoprotein U	Q00839	2.1167	0.4623
26	Glutamine–fructose-6-phosphate aminotransferase [isomerizing] 1	Q06210	2.0343	0.4354
27	Pre-mRNA-splicing factor ATP-dependent RNA helicase DHX15	O43143	2.0206	0.3223
28	CAD protein	P27708	2.0017	0.6633
29	40S ribosomal protein S25	P62851	1.9873	0.6190
30	Proteasome subunit beta type-1	P20618	1.9544	0.7694
31	40S ribosomal protein S11	P62280	1.9443	0.7917
32	Fragile X mental retardation syndrome-related protein 2	P51116	1.944	0.5923
33	Splicing factor 3B subunit 3	Q15393	1.9077	0.6512
34	Histone H4	P62805	1.8442	0.7194
35	Alpha-actinin-1	P12814	1.8384	0.3703
36	ADP/ATP translocase 2	P05141	1.7868	0.1213
37	Flotillin-1	O75955	1.7794	0.6426
38	Myosin light polypeptide 6	P60660	1.7529	0.4116
39	60S ribosomal protein L9	P32969	1.7270	0.7266
40	Endoplasmin	P14625	1.6787	0.3869
41	Profilin-1	P07737	1.6764	0.4943
42	RuvB-like 1	Q9Y265	1.6361	0.7342
43	RNA-binding protein with serine-rich domain 1	Q15287	1.5729	0.4592
44	Transitional endoplasmic reticulum ATPase	P55072	1.5659	0.8456
45	Inosine-5'-monophosphate dehydrogenase 2	P12268	1.5315	0.4383
46	Nucleolin	P19338	0.4557	0.7096
47	Nucleophosmin	P06748	0.3698	0.5086
48	High mobility group protein B2	P26583	0.2475	1.6839
49	High mobility group protein B1	P09429	0.1371	1.6267

Table 1 (continued)

No	Protein name	Protein ID	Pep #1/Control	BT1 + Pep #1/Pep #1
50	Small nuclear ribonucleoprotein Sm D1	P62314	0.1265	2.4964
51	Acidic leucine-rich nuclear phosphoprotein 32 family member A	P39687	0.0761	10.3314

downregulated after Pep #1 stimulation (fold change > 1.5, p value < 0.05, Table S1). Meanwhile, 79 proteins were upregulated and 41 proteins were downregulated upon the combination treatment of Pep #1 and Bantag-1 (fold change > 1.5, p value < 0.05, Table S2). In addition, 128 proteins were upregulated and 36 proteins were downregulated after Bantag-1 inhibition (fold change > 1.5, p value < 0.05, Table S3).

In particular, 51 proteins were systematically dysregulated upon different stimulations (Table 1). Among them, 45 proteins were first upregulated in Pep #1 treated group and further downregulated in BT1 + Pep #1 treated group, such as insulin receptor substrate 4, alpha-actinin-1, myosin light polypeptide 6, and profilin-1. On the other hand, another 6 proteins were first upregulated in Pep #1 treated group and further downregulated in BT1 + Pep #1 treated group, including nucleolin, small nuclear ribonucleoprotein Sm D1, and acidic leucine-rich nuclear phosphoprotein 32 family member A. As shown in Fig. 4c, according to the KEGG pathway analysis of these 51 proteins, signal pathways related to BRS-3 and EVs were identified, including insulin signaling pathway, type 2 diabetes mellitus, proteasome, and regulation of actin cytoskeleton. Therefore, when BRS-3 was activated or inhibited, it caused systematic changes to the cells and lead to the dysregulation of the proteome of released EVs.

RhoA signaling is necessary for EVs secretion

IPA was performed for these 51 proteins (Table 1) to reveal key pathways for EVs secretion. In total, 41 pathways showed significant difference upon treatment, and the top fifteen pathways are listed in Table 2. Specifically, integrin-linked kinase (ILK) signaling acted as an adaptor and mediator signaling linking the extracellular matrix with downstream signaling pathways [30], and sirtuin signaling pathway played important roles in cell fate determination of mesenchymal stem cells [31]. Among these significant pathways, actin cytoskeleton signaling and RhoA signaling pathways were related to EVs secretion, according to a previous report [32]. As shown in Fig. 5a, there were overlapping proteins between actin cytoskeleton signaling and RhoA signaling pathways. In particular, four proteins identified in our proteomics analysis were related to these two pathways. We, therefore, normalized their iBAQ values. Indeed, they were upregulated after stimulation by Pep #1 and downregulated after inhibition by Bantag-1 (Fig. 5b).

Since RhoA/Rho-associated protein kinase (ROCK) signaling pathway promotes tumor cell-derived microvesicles' biogenesis [33], we investigated the necessity of RhoA activation for the release of EVs. We treated HEK293-BRS-3 cells with ROCK I/II inhibitor Y-27632 for RhoA signaling pathway, and used ZetaView to measure the concentration and size distribution of their secreted EVs. As shown in Fig. 5c, after HEK293-BRS-3 cells were stimulated by Pep #1, the amount of cell secreted EVs increased significantly. Conversely, after Y-27632 was added to inhibit RhoA signaling pathway, the amount of cell secreted EVs was significantly reduced. When Pep #1 and Y-27632 were sequentially incubated with HEK293-BRS-3 cells, the secretion of EVs was dramatically inhibited, and the amount of EVs was decreased by about one-third. Meanwhile, there was no size change of EVs for these different treatment groups (data not shown). Therefore, through proteomics analysis of EVs and bioinformatics analysis, we found that RhoA signaling pathway was involved in EVs secretion. According to the verification experiments, we demonstrated that activation of BRS-3 enhanced the RhoA signaling pathway, which in turn promoted the secretion of EVs from HEK293-BRS-3 cells.

Discussion

GPCRs are plasma membrane proteins that spend most of their lifecycle on the cell surface. They can be activated by plentiful stimuli, such as neurotransmitters, peptides, ions, lipids, and even light [34]. After being activated, GPCRs have two classic destinies: recycled to cell membrane, or degraded. Besides, with the in-depth research of EVs, few studies have shown that GPCRs could be sorted into EVs and further delivered to recipient cells. In particular, these re-used GPCRs are functional in the recipient cells. In this study, we aim to demonstrate whether this new fate applies to the orphan GPCR receptor, BRS-3, which plays important roles in obesity, diabetes, and lung cancer [35, 36]. Our results confirmed that BRS-3 could be packed into EVs, and then released to the microenvironment. These EVs as well as their carried receptor BRS-3 could be further absorbed by the recipient cells. Especially, the BRS-3 from the donor

Table 2 Top 15 enriched pathways from IPA analysis after BRS-3 activation

No	Ingenuity Canonical Pathways	*p* value	Molecules	Protein ID	Protein name
1	DNA Double-Strand Break Repair by Non-Homologous End Joining	2.818E−08	PARP1	P09874	Poly [ADP-ribose] polymerase 1
			PRKDC	P78527	DNA-dependent protein kinase catalytic subunit
			XRCC5	P13010	X-ray repair cross-complementing protein 5
			XRCC6	P12956	X-ray repair cross-complementing protein 6
2	Sirtuin signaling pathway	0.0000562	PARP1	P09874	Poly [ADP-ribose] polymerase 1
			PRKDC	P78527	DNA-dependent protein kinase catalytic subunit
			SF3A1	Q15459	Splicing factor 3A subunit 1
			SLC25A5	P05141	ADP/ATP translocase 2
			XRCC5	P13010	X-ray repair cross-complementing protein 5
			XRCC6	P12956	X-ray repair cross-complementing protein 6
3	Spliceosomal Cycle	0.0002188	DHX15	O43143	Pre-mRNA-splicing factor ATP-dependent RNA helicase DHX15
			SF3A1	Q15459	Splicing factor 3A subunit 1
			SF3B3	Q15393	Splicing factor 3B subunit 3
4	Telomere Extension by Telomerase	0.0005754	XRCC5	P13010	X-ray repair cross-complementing protein 5
			XRCC6	P12956	X-ray repair cross-complementing protein 6
5	Granzyme B Signaling	0.0006607	PARP1	P09874	Poly [ADP-ribose] polymerase 1
			PRKDC	P78527	DNA-dependent protein kinase catalytic subunit
6	Granzyme A Signaling	0.0007413	ANP32A	P39687	Acidic leucine-rich nuclear phosphoprotein 32 family member A
			HMGB2	P26583	High mobility group protein B2
7	ILK Signaling	0.0011482	ACTN1	P12814	Alpha-actinin-1
			IRS4	O14654	Insulin receptor substrate 4
			LIMS1	P48059	LIM and senescent cell antigen-like-containing domain protein 1
			MYL6	P60660	Myosin light polypeptide 6
8	Integrin signaling	0.0014454	ACTN1	P12814	Alpha-actinin-1
			LIMS1	P48059	LIM and senescent cell antigen-like-containing domain protein 1
			PFN1	P07737	Profilin-1
			PPP1CB	P62140	Serine/threonine-protein phosphatase PP1-beta catalytic subunit
9	EIF2 Signaling	0.0016218	PPP1CB	P62140	Serine/threonine-protein phosphatase PP1-beta catalytic subunit
			RPL9	P32969	60S ribosomal protein L9
			RPS25	P62851	40S ribosomal protein S25
10	Role of p14/p19ARF in Tumor Suppression	0.0020417	NPM1	P06748	Nucleophosmin
			SF3A1	Q15459	Splicing factor 3A subunit 1
11	Regulation of Actin-based Motility by Rho	0.0022908	MYL6	P60660	Myosin light polypeptide 6
			PFN1	P07737	Profilin-1
			PPP1CB	P62140	Serine/threonine-protein phosphatase PP1-beta catalytic subunit
12	Estrogen Receptor Signaling	0.0025119	HSP90B1	P14625	Endoplasmin
			MYL6	P60660	Myosin light polypeptide 6
			PDIA3	P30101	Protein disulfide-isomerase A3
			PPP1CB	P62140	Serine/threonine-protein phosphatase PP1-beta catalytic subunit
			PRKDC	P78527	DNA-dependent protein kinase catalytic subunit
13	Actin Cytoskeleton Signaling	0.0025704	ACTN1	P12814	Alpha-actinin-1
			MYL6	P60660	Myosin light polypeptide 6
			PFN1	P07737	Profilin-1
			PPP1CB	P62140	Serine/threonine-protein phosphatase PP1-beta catalytic subunit

Table 2 (continued)

No	Ingenuity Canonical Pathways	*p* value	Molecules	Protein ID	Protein name
14	RhoA Signaling	0.0030903	MYL6	P60660	Myosin light polypeptide 6
			PFN1	P07737	Profilin-1
			PPP1CB	P62140	Serine/threonine-protein phosphatase PP1-beta catalytic subunit
15	tRNA Charging	0.0037154	LARS1	Q9P2J5	Leucine–tRNA ligase
			TARS1	P26639	Threonine–tRNA ligase 1

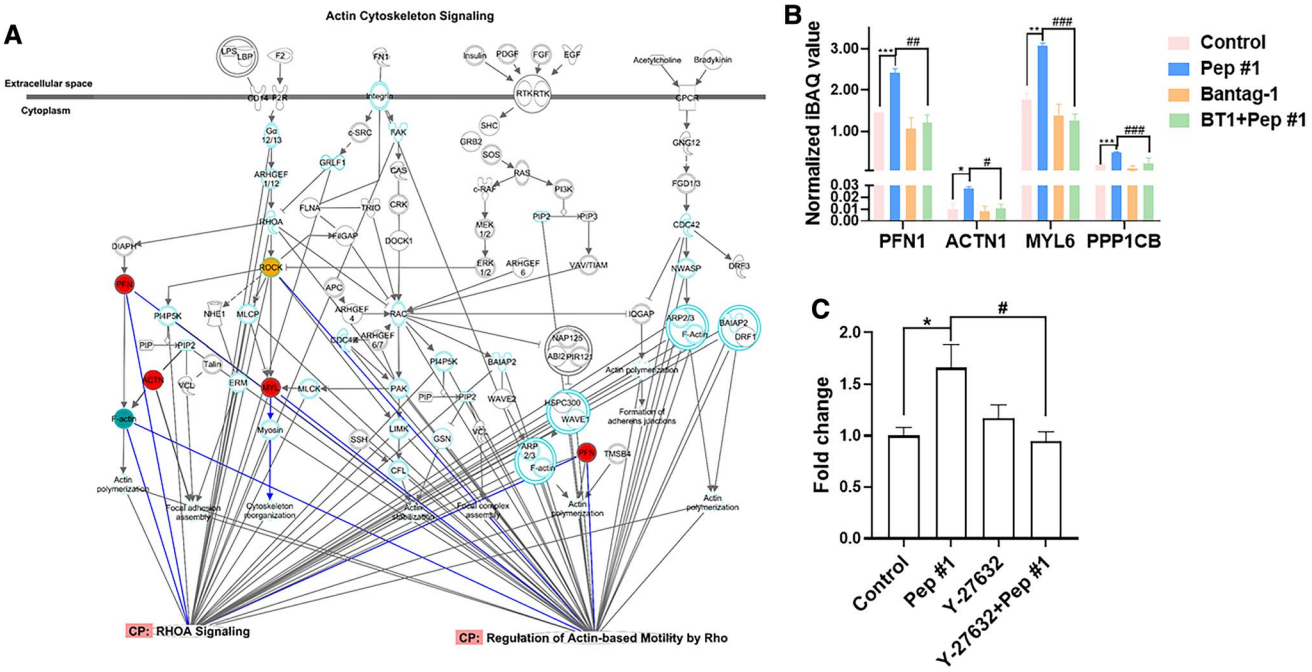

Fig. 5 Inhibition of the RhoA pathway suppressed the secretion of EVs. **a** The major proteins involved in the actin cytoskeleton signaling, regulation of actin-based motility by Rho, and RhoA signaling pathways. The blue circles indicate the proteins that overlapped between the two pathways. The red circles indicate the identified proteins. CP: Canonical Pathway. **b** Changes of four representative proteins related to actin cytoskeleton signaling and RhoA signaling pathways from different treatments. **c** Fold change of EVs from HEK293-BRS-3 cells with different treatments by NTA ($n=7$). *, $p<0.05$, **, $p<0.01$, ***, $p<0.001$ versus control; #, $p<0.05$, ##, $p<0.01$, ###, $p<0.001$ versus BT1 + Pep #1 by *t* test

cells secreted EVs was found to be functional in the recipient cells.

The new fate that GPCRs can be sorted into EVs is closely related to cancer metastasis [10]. It has been reported that exosomes from high lymph node metastatic mouse hepatocarcinoma cells contain CXC chemokine recepter-4 (CXCR4), which could promote the migration and invasion of low metastatic potential cells [37]. BRS-3 is generally overexpressed in human tumors, like lung cancer [38]. In some lung cancer cell lines, the activation of BRS-3 stimulates cell growth by EGFR transactivation [36]. BRS-3 activation may also increase the glucose-stimulated insulin secretion in insulinoma cell lines across multiple species [39, 40]. Moreover, in skeletal muscle cells from patients with obesity and type 2 diabetes, BRS-3's agonist significantly increased the phosphorylation levels of MAPK, p90RSK1, protein kinase B and p70s6K, as well as glucose transport [35]. These studies suggest that BRS-3 may serve as a therapeutic target in lung cancer, obesity, or diabetes. In addition, EVs-carried BRS-3 is a promising biomarker for the detection of these diseases. We also revealed that the BRS-3 transferred by EVs was functional in the recipient cells. Further research is warranted to investigate whether the EVs secreted from lung cancer cells or patient tissues contain BRS-3, and promote the proliferation and metastasis of recipient cells.

In this study, after stimulation or specific inhibition of BRS-3, the protein profiles of the EVs secreted by

HEK293-BBRS-3 cells were significant changed. In total, 51 EVs proteins were found to be systematically dysregulated. Using KEGG pathway analysis of these proteins, we found BRS-3 related pathways, such as type 2 diabetes mellitus [35], insulin signaling pathway [41], and calcium signaling pathway [36], were significantly altered. EVs related pathways were also identified, such as proteasome [42], protein processing in endoplasmic reticulum [43], and regulation of actin cytoskeleton [32]. A few significantly changed proteins were associated with EVs' generation, such as profilin-1, alpha-actinin-1, and myosin light polypeptide 6. In addition, several dysregulated proteins were also involved in BRS-3, such as protein disulfide-isomerase A3 which was related to obesity [44], and serine/threonine-protein phosphatase PP1-beta catalytic subunit which was related to ERK signaling [45]. Furthermore, IPA analysis was performed to analyze differentially expressed proteins of EVs from different treatments of HEK293-BRS-3 cells. The "Canonical pathway" enrichment analysis showed that these proteins were associated with actin cytoskeleton signaling, RhoA signaling, sirtuin signaling pathway, ILK signaling, etc. They were found to play important roles in cell motility, differentiation, cell proliferation, as well as in cancers and inflammation [46–48]. It had also been reported that GPCRs and their downstream signaling components contributed to EVs biogenesis and secretion, which are involved in cAMP and protein kinase A signaling pathways [49, 50], Rag small GTPases and mammalian target of rapamycin complex 1 (mTORC1) kinase [51], Rho family GTPases-regulated F-actin formation [52], and Rho signaling and actomyosin cytoskeleton rearrangements [33, 53]. In our previous study, activation of BRS-3 was also found to promote the mTORC1 pathway [25]. In this study, we focused on the RhoA signaling pathway. After using the RhoA signaling inhibitor-Y27632, the amount of EVs secreted by the HEK293-BRS-3 cells were reduced significantly, though the cells were activated. These results were consistent with that of the IPA analysis, which indicated that proteomics combined with bioinformatics analysis could assist us to find functionally significant pathways. Further research is warranted to establish the link between these proteins and EVs biogenesis. It is also necessary to investigate how EVs are fused into the recipient cells, and how their carried BRS-3 is released in the recipient cells.

Conclusion

Our results demonstrated that the secretion of EVs was significantly increased after the HEK293-BRS-3 cells were stimulated by its agonist. However, specific antagonist significantly inhibited the amount of EVs secreted by the HEK293-BRS-3 cells. More importantly, these secreted EVs contained BRS-3, which could be further transferred to the recipient cells and function in the recipient cells. Collectively, our studies revealed a new fate for BRS-3 and revealed that the secretion of EVs from HEK293-BRS-3 was partially regulated by RhoA signaling pathway.

Supplementary Information The online version contains supplementary material available at https://doi.org/10.1007/s00018-021-04114-z.

Author contributions ZYW, LHW, and HYW performed the experiments and analyzed the data. YZ and HX directed the project and wrote the manuscript. All authors read and approved the final manuscript.

Funding This work was supported by grants from the Natural Science Foundation of Shanghai (No. 21ZR1433200, No. 19ZR1427800), the National Key Research and Development Program of China (No. 2017YFC1200204), the National Natural Science Foundation of China (No. 21675110), and the Key Scientific Project of Shanghai Jiao Tong University (No. TMSK-2020–130, No. YG2017MS80).

Data availability The mass spectrometry proteomics data and the search data by MaxQuant (version 1.6.1.0) have been deposited to the ProteomeXchange Consortium (http://www.ebi.ac.uk/pride/archive/) via the PRIDE partner repository with the dataset identifier PXD027980.

Code availability Not applicable.

Declarations

Conflict of interest The authors declare no competing financial interests.

References

1. van Niel G, D'Angelo G, Raposo G (2018) Shedding light on the cell biology of extracellular vesicles. Nat Rev Mol Cell Biol 19:213–228. https://doi.org/10.1038/nrm.2017.125
2. Théry C, Witwer KW, Aikawa E, Alcaraz MJ, Anderson JD et al (2018) Minimal information for studies of extracellular vesicles 2018 (MISEV2018): a position statement of the International Society for Extracellular Vesicles and update of the MISEV2014 guidelines. J Extracell Vesicles 7:1535750. https://doi.org/10.1080/20013078.2018.1535750
3. Yáñez-Mó M, Siljander PR, Andreu Z, Zavec AB, Borràs FE et al (2015) Biological properties of extracellular vesicles and their physiological functions. J Extracell Vesicles 4:27066. https://doi.org/10.3402/jev.v4.27066
4. Raposo G, Stoorvogel W (2013) Extracellular vesicles: exosomes, microvesicles, and friends. J Cell Biol 200:373–383. https://doi.org/10.1083/jcb.201211138
5. Wolf P (1967) The nature and significance of platelet products in human plasma. Br J Haematol 13:269–288. https://doi.org/10.1111/j.1365-2141.1967.tb08741.x
6. Tkach M, Théry C (2016) Communication by extracellular vesicles: where we are and where we need to go. Cell 164:1226–1232. https://doi.org/10.1016/j.cell.2016.01.043

7. Wu P, Zhang B, Ocansey DKW, Xu W, Qian H (2021) Extracellular vesicles: a bright star of nanomedicine. Biomaterials 269:120467. https://doi.org/10.1016/j.biomaterials.2020.120467
8. Abhange K, Makler A, Wen Y, Ramnauth N, Mao W et al (2021) Small extracellular vesicles in cancer. Bioact Mater 6:3705–3743. https://doi.org/10.1016/j.bioactmat.2021.03.015
9. Pocsfalvi G, Stanly C, Vilasi A, Fiume I, Capasso G et al (2016) Mass spectrometry of extracellular vesicles. Mass Spectrom Rev 35:3–21. https://doi.org/10.1002/mas.21457
10. Isola AL, Chen S (2016) Exosomes: the link between GPCR activation and metastatic potential? Front Genet. https://doi.org/10.3389/fgene.2016.00056
11. Rosenbaum DM, Rasmussen SG, Kobilka BK (2009) The structure and function of G-protein-coupled receptors. Nature 459:356–363. https://doi.org/10.1038/nature08144
12. Hauser AS, Attwood MM, Rask-Andersen M, Schiöth HB, Gloriam DE (2017) Trends in GPCR drug discovery: new agents, targets and indications. Nat Rev Drug Discov 16:829–842. https://doi.org/10.1038/nrd.2017.178
13. Morri M, Sanchez-Romero I, Tichy AM, Kainrath S, Gerrard EJ et al (2018) Optical functionalization of human Class A orphan G-protein-coupled receptors. Nat Commun 9:1950. https://doi.org/10.1038/s41467-018-04342-1
14. Xiao C, Reitman ML (2016) Bombesin-like receptor 3: physiology of a functional orphan. Trends Endocrinol Metab 27:603–605. https://doi.org/10.1016/j.tem.2016.03.003
15. Fathi Z, Corjay MH, Shapira H, Wada E, Benya R et al (1993) BRS-3: a novel bombesin receptor subtype selectively expressed in testis and lung carcinoma cells. J Biol Chem 268:5979–5984
16. Jensen RT, Battey JF, Spindel ER, Benya RV (2008) International Union of Pharmacology. LXVIII. Mammalian bombesin receptors: nomenclature, distribution, pharmacology, signaling, and functions in normal and disease states. Pharmacol Rev 60:1–42. https://doi.org/10.1124/pr.107.07108
17. Weber HC (2009) Regulation and signaling of human bombesin receptors and their biological effects. Curr Opin Endocrinol Diabetes Obes 16:66–71. https://doi.org/10.1097/med.0b013e32831cf5aa
18. Piñol RA, Zahler SH, Li C, Saha A, Tan BK et al (2018) Brs3 neurons in the mouse dorsomedial hypothalamus regulate body temperature, energy expenditure, and heart rate, but not food intake. Nat Neurosci 21:1530–1540. https://doi.org/10.1038/s41593-018-0249-3
19. Li M, Liang P, Liu D, Yuan F, Chen GC et al (2019) Bombesin receptor subtype-3 in human diseases. Arch Med Res 50:463–467. https://doi.org/10.1016/j.arcmed.2019.11.004
20. Ramos-Alvarez I, Lee L, Mantey SA, Jensen RT (2019) Development and characterization of a novel, high-affinity, specific, radiolabeled ligand for BRS-3 receptors. J Pharmacol Exp Ther 369:454–465. https://doi.org/10.1124/jpet.118.255141
21. von Zastrow M (2003) Mechanisms regulating membrane trafficking of G protein-coupled receptors in the endocytic pathway. Life Sci 74:217–224. https://doi.org/10.1016/j.lfs.2003.09.008
22. Sorkin A, Von Zastrow M (2002) Signal transduction and endocytosis: close encounters of many kinds. Nat Rev Mol Cell Biol 3:600–614. https://doi.org/10.1038/nrm883
23. Dores MR, Trejo J (2019) Endo-lysosomal sorting of G-protein-coupled receptors by ubiquitin: diverse pathways for G-protein-coupled receptor destruction and beyond. Traffic 20:101–109. https://doi.org/10.1111/tra.12619
24. Pironti G, Strachan RT, Abraham D, Mon-Wei Yu S, Chen M et al (2015) Circulating exosomes induced by cardiac pressure overload contain functional angiotensin II type 1 receptors. Circulation 131:2120–2130. https://doi.org/10.1161/circulationaha.115.015687
25. Dong L, Zhang B, Wu L, Shang Z, Liu S et al (2020) Proteomics analysis of cellular BRS3 receptor activation reveals potential mechanism for signal transduction and cell proliferation. J Proteome Res 19:1513–1521. https://doi.org/10.1021/acs.jproteome.9b00760
26. Qiao Z, Zhang Y, Ge M, Liu S, Jiang X et al (2019) Cancer cell derived small extracellular vesicles contribute to recipient cell metastasis through promoting HGF/c-met pathway. Mol Cell Proteomics 18:1619–1629. https://doi.org/10.1074/mcp.RA119.001502
27. Sun Y, Liu S, Qiao Z, Shang Z, Xia Z et al (2017) Systematic comparison of exosomal proteomes from human saliva and serum for the detection of lung cancer. Anal Chim Acta 982:84–95. https://doi.org/10.1016/j.aca.2017.06.005
28. Guan XM, Chen H, Dobbelaar PH, Dong Y, Fong TM et al (2010) Regulation of energy homeostasis by bombesin receptor subtype-3: selective receptor agonists for the treatment of obesity. Cell Metab 11:101–112. https://doi.org/10.1016/j.cmet.2009.12.008
29. Moreno P, Mantey SA, Nuche-Berenguer B, Reitman ML, González N et al (2013) Comparative pharmacology of bombesin receptor subtype-3, nonpeptide agonist MK-5046, a universal peptide agonist, and peptide antagonist Bantag-1 for human bombesin receptors. J Pharmacol Exp Ther 347:100–116. https://doi.org/10.1124/jpet.113.206896
30. Almasabi S, Ahmed AU, Boyd R, Williams BRG (2021) A potential role for integrin-linked kinase in colorectal cancer growth and progression via regulating senescence and immunity. Front Genet 12:638558. https://doi.org/10.3389/fgene.2021.638558
31. Chen H, Liu X, Chen H, Cao J, Zhang L et al (2014) Role of SIRT1 and AMPK in mesenchymal stem cells differentiation. Ageing Res Rev 13:55–64. https://doi.org/10.1016/j.arr.2013.12.002
32. Bebelman MP, Crudden C, Pegtel DM, Smit MJ (2020) The convergence of extracellular vesicle and GPCR biology. Trends Pharmacol Sci 41:627–640. https://doi.org/10.1016/j.tips.2020.07.001
33. Sedgwick AE, Clancy JW, Olivia Balmert M, D'Souza-Schorey C (2015) Extracellular microvesicles and invadopodia mediate non-overlapping modes of tumor cell invasion. Sci Rep 5:14748. https://doi.org/10.1038/srep14748
34. Pierce KL, Premont RT, Lefkowitz RJ (2002) Seven-transmembrane receptors. Nat Rev Mol Cell Biol 3:639–650. https://doi.org/10.1038/nrm908
35. González N, Martín-Duce A, Martínez-Arrieta F, Moreno-Villegas Z, Portal-Núñez S et al (2015) Effect of bombesin receptor subtype-3 and its synthetic agonist on signaling, glucose transport and metabolism in myocytes from patients with obesity and type 2 diabetes. Int J Mol Med 35:925–931. https://doi.org/10.3892/ijmm.2015.2090
36. Moreno P, Mantey SA, Lee SH, Ramos-Álvarez I, Moody TW et al (2018) A possible new target in lung-cancer cells: The orphan receptor, bombesin receptor subtype-3. Peptides 101:213–226. https://doi.org/10.1016/j.peptides.2018.01.016
37. Li M, Lu Y, Xu Y, Wang J, Zhang C et al (2018) Horizontal transfer of exosomal CXCR4 promotes murine hepatocarcinoma cell migration, invasion and lymphangiogenesis. Gene 676:101–109. https://doi.org/10.1016/j.gene.2018.07.018
38. Moreno P, Ramos-Álvarez I, Moody TW, Jensen RT (2016) Bombesin related peptides/receptors and their promising therapeutic roles in cancer imaging, targeting and treatment. Expert Opin Ther Targets 20:1055–1073. https://doi.org/10.1517/14728222.2016.1164694
39. Feng Y, Guan XM, Li J, Metzger JM, Zhu Y et al (2011) Bombesin receptor subtype-3 (BRS-3) regulates glucose-stimulated insulin secretion in pancreatic islets across multiple species. Endocrinology 152:4106–4115. https://doi.org/10.1210/en.2011-1440

40. Ramos-Álvarez I, Martín-Duce A, Moreno-Villegas Z, Sanz R, Aparicio C et al (2013) Bombesin receptor subtype-3 (BRS-3), a novel candidate as therapeutic molecular target in obesity and diabetes. Mol Cell Endocrinol 367:109–115. https://doi.org/10.1016/j.mce.2012.12.025
41. González N, Moreno P, Jensen RT (2015) Bombesin receptor subtype 3 as a potential target for obesity and diabetes. Expert Opin Ther Targets 19:1153–1170. https://doi.org/10.1517/14728222.2015.1056154
42. Marcoux G, Laroche A, Hasse S, Bellio M, Mbarik M et al (2021) Platelet EVs contain an active proteasome involved in protein processing for antigen presentation via MHC-I molecules. Blood. https://doi.org/10.1182/blood.2020009957
43. Wu CH, Silvers CR, Messing EM, Lee YF (2019) Bladder cancer extracellular vesicles drive tumorigenesis by inducing the unfolded protein response in endoplasmic reticulum of nonmalignant cells. J Biol Chem 294:3207–3218. https://doi.org/10.1074/jbc.RA118.006682
44. Alfadda AA, Benabdelkamel H, Masood A, Moustafa A, Sallam R et al (2013) Proteomic analysis of mature adipocytes from obese patients in relation to aging. Exp Gerontol 48:1196–1203. https://doi.org/10.1016/j.exger.2013.07.008
45. Young LC, Hartig N, Boned Del Río I, Sari S, Ringham-Terry B et al (2018) SHOC2-MRAS-PP1 complex positively regulates RAF activity and contributes to Noonan syndrome pathogenesis. Proc Natl Acad Sci USA 115:10576–10585. https://doi.org/10.1073/pnas.1720352115
46. Wang Q, Symes AJ, Kane CA, Freeman A, Nariculam J et al (2010) A novel role for Wnt/Ca2+ signaling in actin cytoskeleton remodeling and cell motility in prostate cancer. PLoS ONE 5:126–126
47. Yu OM, Brown JH (2015) GPCR and RhoA-stimulated transcriptional responses mediating inflammation. Differen Cell Prolif Mol Pharmacol 88(1):171–180. https://doi.org/10.1124/mol.115.097857
48. Pang MF, Stallings-Mann M, Siedlik MJ, Han S, Nelson CM (2016) ILK as a signaling nexus for induction of breast cancer stem cells in response to tissue stiffness and hypoxia. Eur J Cancer 61:S40–S40
49. Glebov K, Löchner M, Jabs R, Lau T, Merkel O et al (2015) Serotonin stimulates secretion of exosomes from microglia cells. Glia 63:626–634. https://doi.org/10.1002/glia.22772
50. Islam A, Jones H, Hiroi T, Lam J, Zhang J et al (2008) cAMP-dependent protein kinase A (PKA) signaling induces TNFR1 exosome-like vesicle release via anchoring of PKA regulatory subunit RIIbeta to BIG2. J Biol Chem 283:25364–25371. https://doi.org/10.1074/jbc.M804966200
51. Gan L, Seki A, Shen K, Iyer H, Han K et al (2019) The lysosomal GPCR-like protein GPR137B regulates Rag and mTORC1 localization and activity. Nat Cell Biol 21:614–626. https://doi.org/10.1038/s41556-019-0321-6
52. Kajimoto T, Mohamed NNI, Badawy SMM, Matovelo SA, Hirase M et al (2018) Involvement of Gβγ subunits of G(i) protein coupled with S1P receptor on multivesicular endosomes in F-actin formation and cargo sorting into exosomes. J Biol Chem 293:245–253. https://doi.org/10.1074/jbc.M117.808733
53. Das K, Prasad R, Singh A, Bhattacharya A, Roy A et al (2018) Protease-activated receptor 2 promotes actomyosin dependent transforming microvesicles generation from human breast cancer. Mol Carcinog 57:1707–1722. https://doi.org/10.1002/mc.22891